Journal of Alloys and Compounds 509 (2011) 9951–9958

Contents lists available at ScienceDirect

Journal of Alloys and Compounds

journal homepage: www.elsevier.com/locate/jallcom

Gas-tungsten arc welding of AZ91 magnesium alloy

K.N. Braszczyńska-Malik[a,*], M. Mróz[b]

[a] Czestochowa University of Technology, Institute of Materials Engineering, Al. Armii Krajowej 19, 42-200 Czestochowa, Poland
[b] Rzeszow University of Technology, Department of Casting and Welding, St. W. Pola 2, 35-959 Rzeszow, Poland

ARTICLE INFO

Article history:
Received 29 December 2010
Accepted 30 July 2011
Available online 4 August 2011

Keywords:
Magnesium alloy
Arc and melting efficiency
Microstructure
Arc-tungsten gas welding

ABSTRACT

The gas-tungsten arc (GTA) welding behaviors of the commercial AZ91 magnesium alloy were examined in terms of process efficiencies and microstructure characteristics. This study focused on the effects of GTA welding process parameters (like welding current in the range of 100/300 A and welding speed in the range of 3.33/13.33 mm/s) on energy absorption by the substrate material. The dependences of arc and welding efficiency on the used process parameters were presented. The measurements revealed that the arc efficiency values ranged from 0.63 to 0.88. Melting efficiency was found to rise with both increasing welding current and speed. The analyses revealed a strong influence of the GTA welding process on the width and depth of the fusion zone and also on the refinement of the microstructure in the fusion zone. The results of dendrite arm size (DAS) measurements were presented. Additionally, the presence of a partially melted zone (PMZ) was disclosed.

1. Introduction

The AZ91 (Mg–Al–Zn) alloy is the most widely used magnesium alloy exhibiting a good combination of high strength at room temperature, good castability and excellent corrosion resistance [1–4]. A dendritic microstructure is typical for the as-cast AZ91 magnesium alloy, which is characterized by very heavy segregation of the alloying elements. A non-equilibrium solidification condition caused the formation of large crystals of a solid solution of Al in Mg – depleted in aluminium – (an α phase with a hexagonal closely-packed, hcp, structure) and pushing the Al admixture away into interdendritical spaces. In the last stage of solidification, the α + γ binary eutectic is formed at 710 K. The γ-phase (called also β-phase) is an intermetallic compound with a stoichiometric composition of $Mg_{17}Al_{12}$ (at 43.95 wt.% Al) and an α-Mn-type cubic unit cell [2,5–7]. In comparison to binary Mg–Al, new phases do not appear in commercial ternary alloys with zinc (like AZ91) when the Al to Zn ratio is larger than 3:1. In this case, the zinc substitutes aluminium in the γ-$Mg_{17}Al_{12}$ phase, creating a ternary intermetallic compound $Mg_{17}Al_{11.5}Zn_{0.5}$ or $Mg_{17}(Al, Zn)_{12}$ type [3,8]. In the AZ91 alloy, an Al_8Mn_5 intermetallic phase is also present due to the manganese addition to the alloy [9].In commercial hypoeutectic Mg–Al alloys (with aluminium contents less than about 10 wt.% Al), the eutectic exhibited morphologies that are generally referred to as fully or partially divorced. Generally, in Mg–Al alloys the eutectic tends to become more divorced with an increasing cooling rate but its morphology also depends on the location of the couple zone and undercooling during solidification [2,4,6,7]. In commercial cast ingots, both types of eutectic are observed depending on local solidification conditions inside the ingot and also on the depth of etching reagent penetration [2]. The two main microstructural constituents (primary α phase and α + γ binary eutectic) have different properties. In typical AZ91 ingots, the Vickers microhardness for the α + γ eutectic regions is about 190 $HV_{0.01}$ whereas for the α phase, it is only 64 $HV_{0.01}$ (the average Brinell hardness for alloy is about 78 HB) [2]. The Young modulus of the γ phase is about 80 GPA whereas of magnesium, it is only 45 GPA [5,10]. Therefore, the morphology, and particularly size, of the microstructural constituents determines the properties of the as-cast AZ91 alloy.

Recently, the welding technology of magnesium alloys, including friction stir welding, tungsten inert gas (TIG) welding, laser hybrid welding or electron-beam welding processes, have been investigated widely [11–20]. One of these methods is also gas-tungsten arc (GTA) welding, which has been used extensively for the advantages of utility and economy (i.e. short processing time, flexibility operation, economy in time, energy and material consumption and processing precision). The GTA welding technique also requires only a low cost for equipment investment. Additionally, GTA welding produces very high quality welds as opposed to other methods, thus minimizing the complicating effects arising from weld defects such as porosity, undercuts and weld spatter. There are several reports describing the influence of GTA welding technology on magnesium behavior [21–30] but those investigations were not concerned with process efficiencies. There are two main dimensionless process efficiencies that can be measured as a

* Corresponding author. Tel.: +48 34 3250 721; fax: +48 34 3250 721.
E-mail address: kacha@wip.pcz.pl (K.N. Braszczyńska-Malik).

0925-8388/$ – see front matter © 2011 Elsevier B.V. All rights reserved.
doi:10.1016/j.jallcom.2011.07.105

Table 1
Chemical composition of AZ91 alloy according to ASTM B93-94.

Chemical composition [wt.%][a]								
Alloy	Al	Zn	Mn	Si max	Fe max	Cu max	Ni max	Others each max
AZ91	8.5/9.5	0.45/0.9	0.17/0.4	0.05	0.005	0.03	0.002	0.02

[a] Mg rest.

function of controllable processing variables, i.e. arc efficiency (η) and melting efficiency (η_m). Arc efficiency is used to describe the ratio of energy that is absorbed by the workpiece over the energy generated by the heat source. For the case of the GTA welding process, arc efficiency can be defined as the ratio of heat absorbed by the workpiece to the incident arc energy. This fraction is always less than the unity because not all of the energy generated by the heat source is absorbed by the welded material. On the other hand, melting efficiency is used to describe the amount of energy that is used to create a molten weld pool from the energy delivered to and absorbed by the workpiece. Only a small portion of the energy is actually used for melting the fusion zone. The rest of it is dissipated to the surrounding area by thermal conductivity. Melting efficiency depends on the process parameters (i.e. arc power and welding speed), heat flow geometry and the base material thermophysical properties. The experimental data obtained from calorimetric methods allowed the evaluation of the real values of both these efficiencies. In the present work, the arc and melting efficiency for the AZ91 magnesium alloy employing different GTA welding process parameters were investigated. Additionally, the influence of GTA welding parameters on microstructure changes was examined.

2. Experimental material and procedures

Commercial ingots of AZ91 magnesium alloy were used as the starting material. The nominated chemical composition of the AZ91 alloy according to the ASTM B93-94 standard is given in Table 1. Welding plates were machined to the size of 250 mm × 50 mm × 15 mm. The gas-tungsten arc (GTA) welding method was conducted by using a Falting 315 AC/DC instrument. A set of 2.4 mm diameter tungsten electrodes were used (WT20 according to the DIN Standard). The shielding gas was helium with a flow rate of 20 l/min. This shielding gas was chosen because helium due to its high first ionization potential (24.6 eV) increases the constant-current voltage and creates a larger fusion zone than argon (15.6 eV) [21]. Investigations were conducted utilizing different welding parameters: 12/15 V voltage, 100/300 A current and 3.33/13.3 mm/s welding speed. The total heat content absorbed by the material (Q_m) was obtained by the calorimetric method using the flow type calorimeter (Fig. 1). The water flow rate was 7.5 l/min. Arc efficiency (η) was obtained from the equation:

$$\eta = \frac{Q_m}{UIt} \tag{1}$$

where U is the welding voltage [V], I – welding current [A], t – time of welding [s].

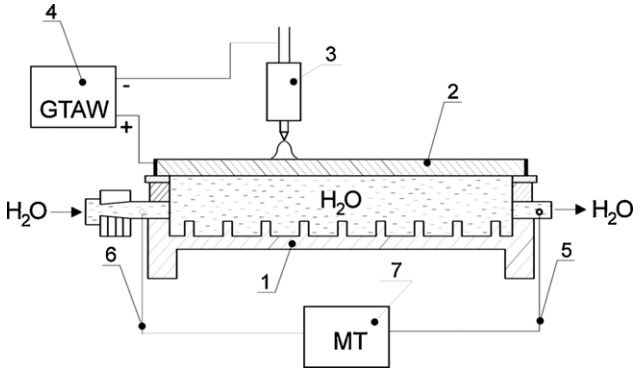

Fig. 1. Equipment for determination of arc efficiency: 1 – flow calorimeter, 2 – sample, 3 – GTA torch, 4 – current source, 5, 6 – thermocouples, 7 – temperature recorder.

Melting efficiency (η_m) was calculated from the relationship:

$$\eta_m = \frac{V_n \rho \left(Q_F + \int_{T_1}^{T_2} c_p \ dT \right)}{Q_m} \tag{2}$$

where V_n – total volume of the fusion zone [cm^3], ρ – density [g/cm^3], T_1 – ambient temperature [K], T_2 – liquidus temperature [K], Q_F – melting heat [J/g], c_p – specific heat [J/g K].

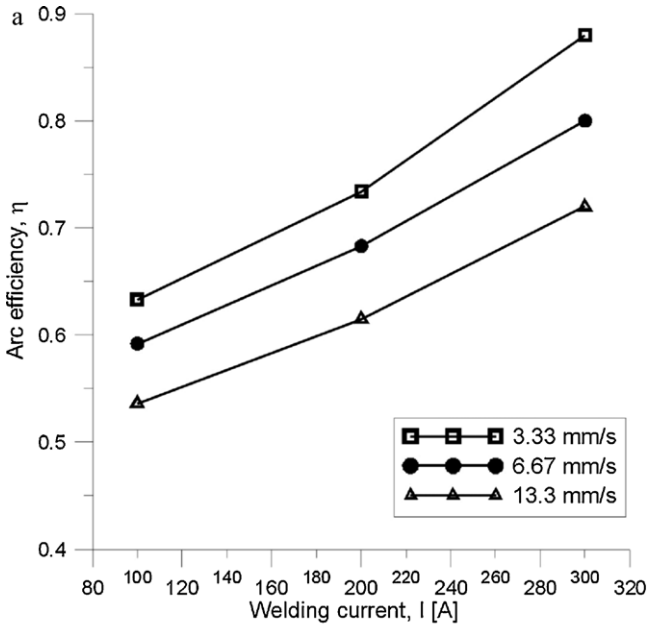

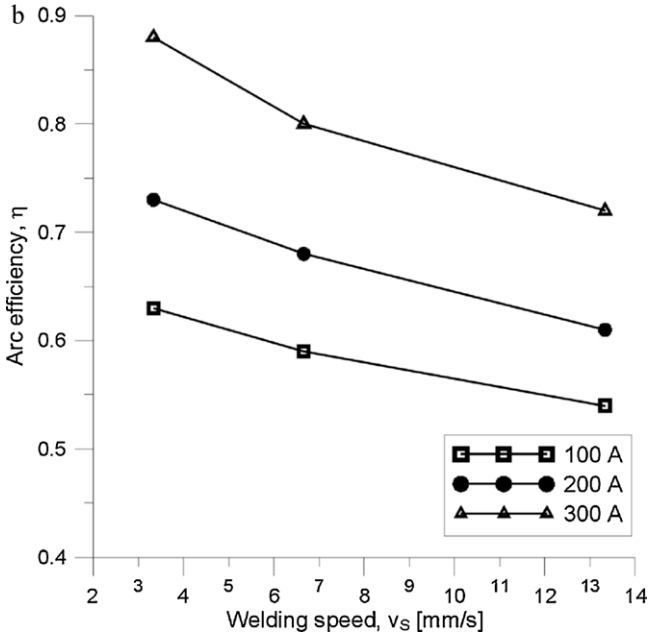

Fig. 2. Influence of welding current (a) and speed (b) on arc efficiency during GTA welding of AZ91 alloy.

Table 2
Applied GTA welding parameters with obtained results of process efficiencies and width and depth of fusion zone.

Welding current, I [A]	Welding speed, v_S [mm/s]	Welding voltage, U [V]	Arc efficiency, η	Melting efficiency, η_m	Width of fusion zone, d_{FZ} [mm]	Depth of fusion zone, h_{FZ} [mm]
100	3.33	12	0.63	0.04	5.78	1.17
200	3.33	13	0.73	0.06	10.12	3.37
300	3.33	15	0.88	0.10	15.18	7.89
100	6.67	12	0.59	0.06	4.80	0.76
200	6.67	13	0.68	0.11	8.68	2.49
300	6.67	15	0.80	0.20	13.43	6.20
100	13.3	12	0.54	0.09	2.95	0.31
200	13.3	13	0.61	0.21	5.92	1.44
300	13.3	15	0.72	0.41	10.00	3.80

The total volume of the fusion zone (V_n) was determined by multiplying the cross-sectional area of the fusion zone by its length. The specimens for measuring the geometry of the fusion zone (they width and depth) and also for microstructure investigations were prepared by standard metallographic procedures including wet prepolishing and polishing with different diamond pastes without contact with water. To reveal the microstructure, the samples were etched in a 1% solution of HNO_3 in C_2H_5OH for about 60 s. The microstructure was observed using light and scanning electron microscopy techniques. In order to determine the influence of the GTA welding process on microstructure changes, the dendrite arm size (DAS) of the base material and the fusion zone was obtained using the linear method as a quotient of the mean distance between the dendrite cross-section centers by the number of arms. The results were obtained from about 120 measurements for each sample.

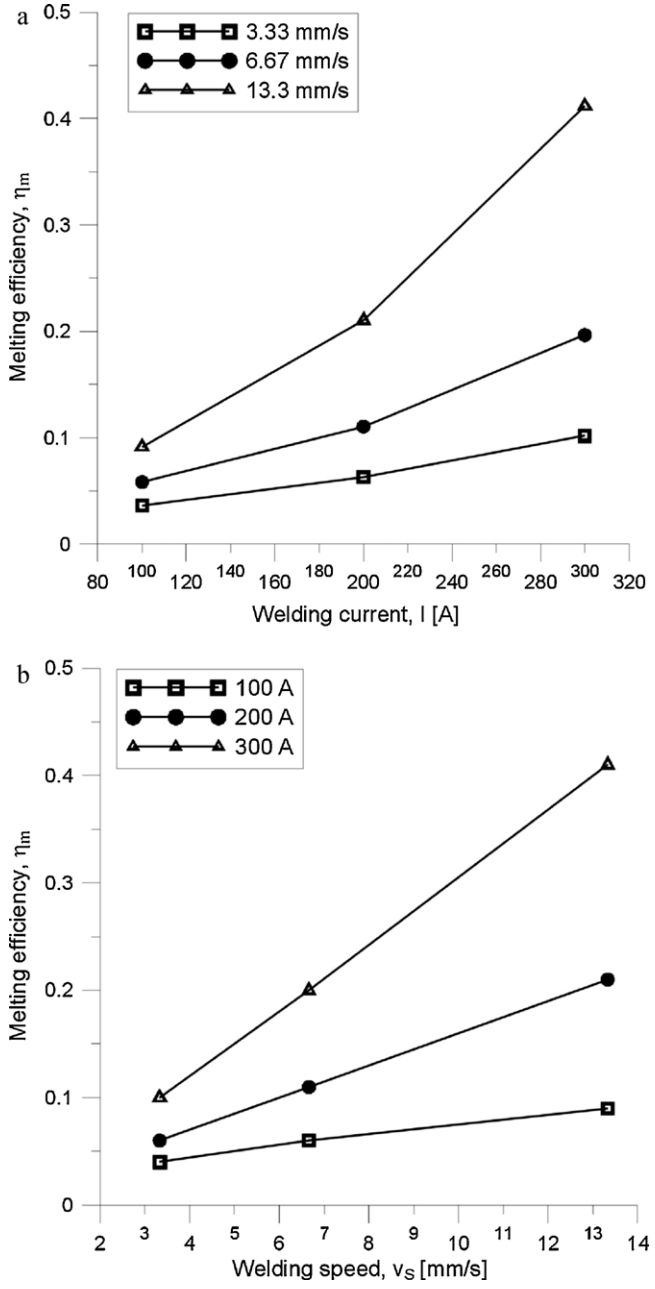

Fig. 3. Influence of welding current (a) and speed (b) on melting efficiency during GTA welding of AZ91 alloy.

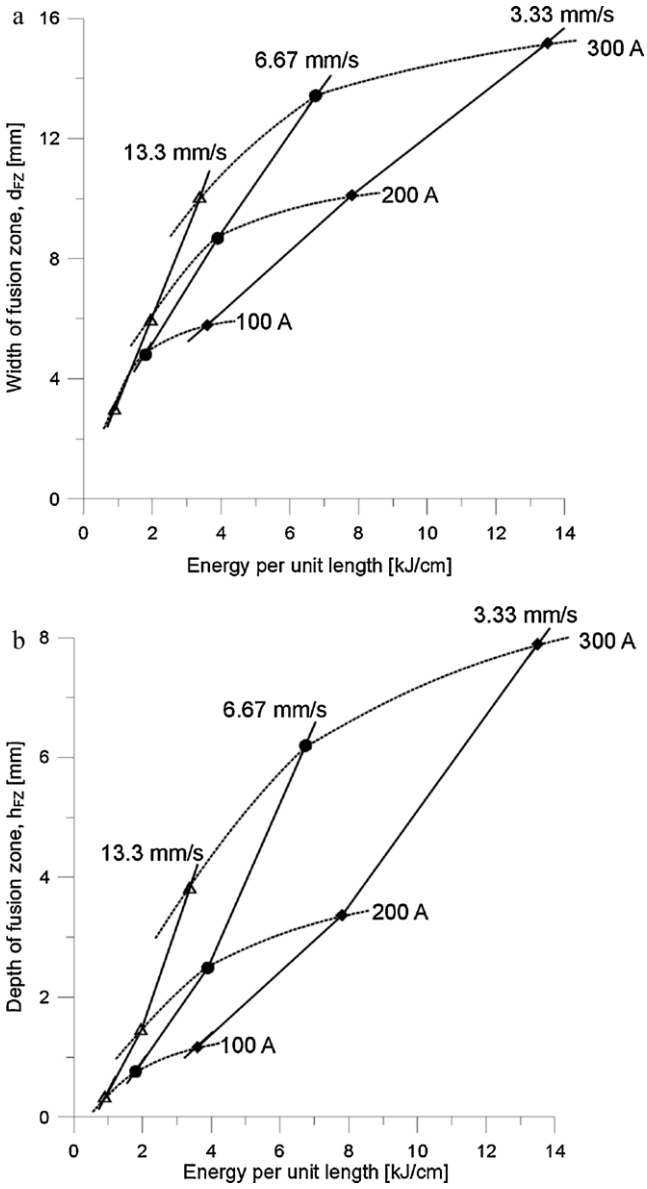

Fig. 4. Width (a) and depth (b) of fusion zone as a function of energy per unit length.

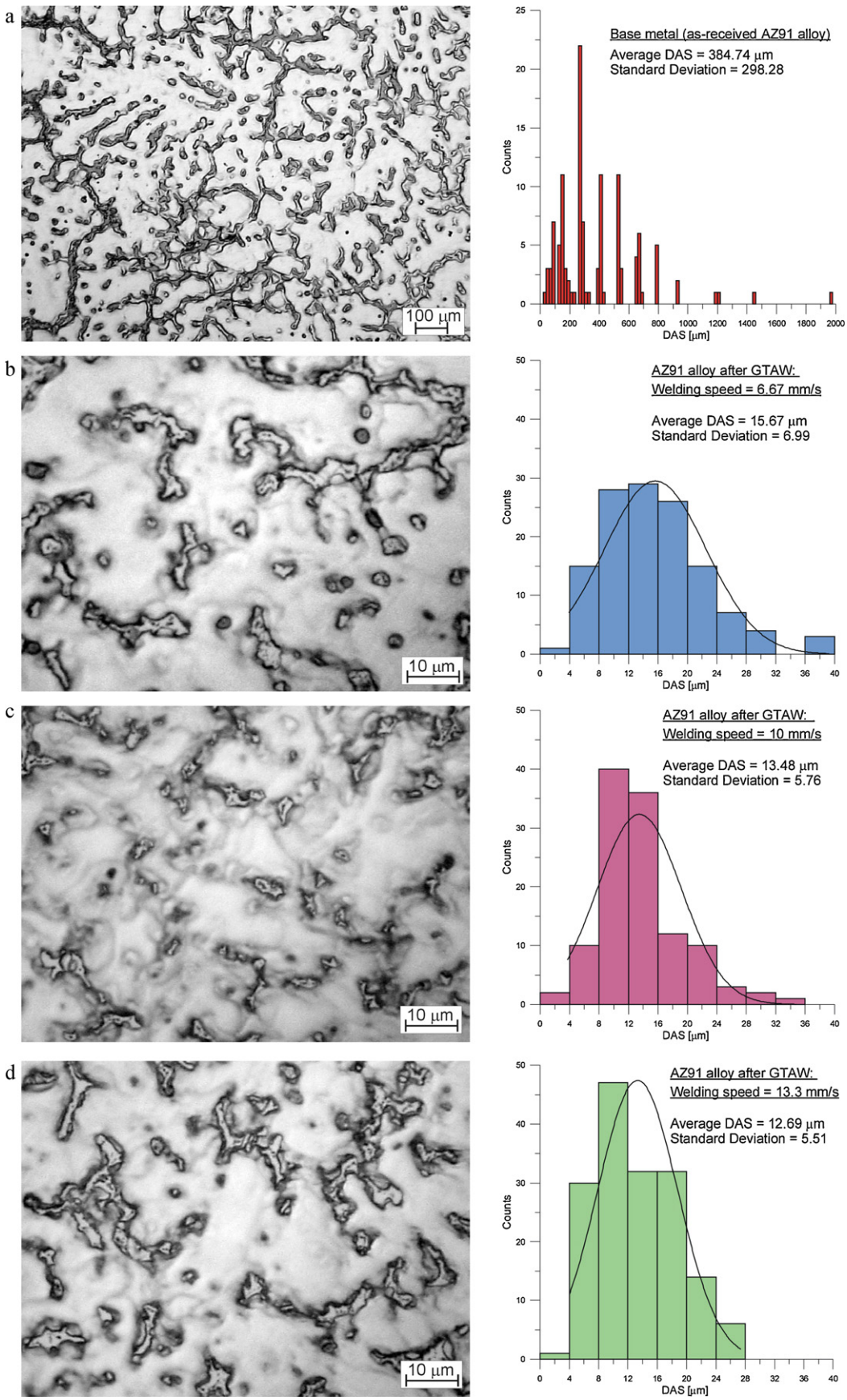

Fig. 5. Microstructure of base metal (a) and fusion zone (b–d) after GTA welding of AZ91 alloy at current of 300 A with corresponding DAS results.

3. Result and discussion

3.1. GTA welding process efficiencies and fusion zone geometry

The values of arc and melting efficiency obtained from the conducted investigations are presented in Table 2. For the GTA welding parameters used in this study, the arc efficiency values ranged between 0.63 (with 100 A current and 3.33 mm/s welding speed) and 0.88 (with 300 A current and 3.33 welding speed). This indicates that 40/10 pct of the arc energy was never transformed to the substrate. Fig. 2a and b presents the arc efficiency as a function of the welding current and speed, respectively. As can be seen from the presented dependences, arc efficiency rose with an increase in welding current and fell with an increase in welding speed. As could be expected, by using a higher welding current or lower welding speed, more heat was absorbed by the workpiece. The effects of the welding current and speed on melting efficiency are displayed in Fig. 3a and b, respectively. In this case, melting efficiency rose with an increase in both the welding current and speed. The maximum value of melting efficiency was 0.41 using a welding current of 300 A and speed of 13.33 mm/s. From the total energy that is transformed to the workpiece, only a small fraction of it was used to create a molten pool. Melting efficiency rose with the increasing rate of energy (i.e. welding power defined as a product of current and voltage) delivered to the material. When the energy was distributed to a localized region at a slower rate (i.e. lower welding power), there was effectively more time available for the energy to be transformed away from the molten region by thermal conduction to the surrounding material. On the other hand when melting occurred at a faster welding speed, less time was available for the heat to be transformed away from the localized melted region. In consequence of this, more total energy was used to create the molten weld pool. Therefore, an increase in welding speed results in an increase in melting efficiency. The obtained kinds of relationships are typical for welding technology.

As should be expected, when arc and melting efficiency increased, the amount of heat introduced to the workpiece increased as well. Therefore, the width and depth of the fusion zone were enlarged. The values of the width and depth of the fusion zone obtained using different GTA welding parameters are presented in Table 2. As can be seen from those results, both the width and depth of the fusion zone increased with an increase in the welding current (at constant welding speed) and fell with an increase in welding speed (at constant welding current). Fusion zone geometry depends obviously on linear energy (i.e. energy per unit length, which is defined as the quantity of energy incident upon the workpiece per unit length and is given by the ratio of input power to welding speed). Therefore, it is clear that if the welding power increases or welding speed decreases, the energy per unit length will rise. Fig. 4a and b presents the width and depth of the fusion zone, respectively, as a function of the energy per unit length for all the GTA welding parameters used in this study. As can be seen, by increasing the energy per unit length, both the geometry parameters of the fusion zone became larger. Hence, a wider fusion zone could be obtained by using a higher welding power or lower welding speed.

3.2. Microstructure analysis

In the presented study, the influence of the GTA welding process on AZ91 alloy microstructure changes was also investigated. Fig. 5 presents the microstructure differences between the base material and fusion zones after GTA welding with a current of 300 A and at different welding speeds. It is visible that the DAS was considerably reduced after GTA welding. The reason for the forming of a fine microstructure was that the rapid cooling induced by good thermal conductivity (51 $W m^{-1} K^{-1}$) and low capacity (1.02 $kJ kg^{-1} K^{-1}$) of the AZ91 magnesium alloy hampered the growth of dendrites in the fusion zone. The differences of the DAS parameter between the samples welded employing different parameters were not so great. For all the investigated fusion zones, the DAS results exhibited Gaussian distribution. The results presented in Fig. 5 show that the DAS (and its standard devotion) of melted material decreased with an increase in welding speed. It is well known, that DAS parameters depend on the solidification conditions, especially the cooling rate. A decrease in welding speed (and the same increase in energy input) results in a decrease in the cooling rate. Moreover, a slower cooling rate during solidification results in a longer time available for primary dendrite growth. Therefore the choice of suitable welding parameters allowed the achievement of different DAS. It should also be noted, that the differences in the cooling rate were too small to exert influence on eutectic morphology. As can be seen from Fig. 5b to d, the eutectic inside the fusion zone had the same morphology in all the samples welded using different process parameters. On the other hand, a lower welding speed created a higher heat input, which resulted in a wider fusion zone (Fig. 4). The influence of the welding speed on both the DAS and depth of the fusion zone is shown in Fig. 6.

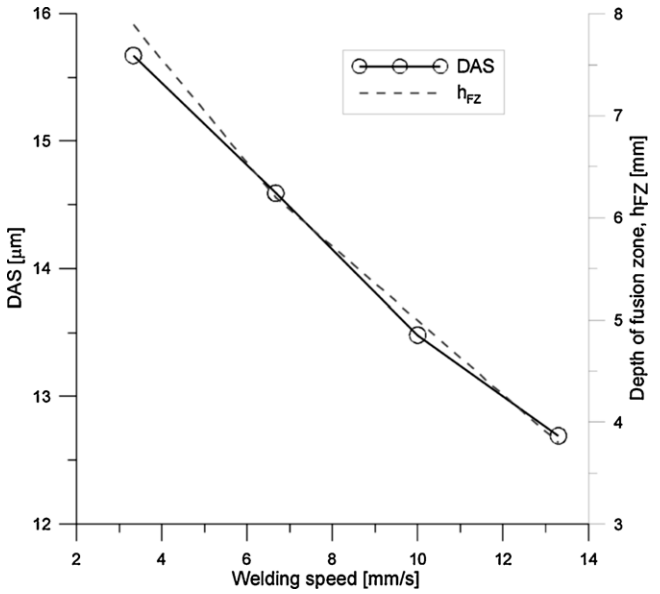

Fig. 6. Dependence of DAS and fusion zone depth on welding speed.

It should also be noted that the low-melting point nature of the eutectic, only 710 K (and also of the γ phase – about 723 K) coupled with the high thermal conductivity and low heat capacity of the AZ91 alloy, lead to the formation of a wide partially melted zone (PMZ), which was located from the fusion boundary to the base metal. For all the samples GTA welded utilizing different process parameters, partially melted zones were observed. The presence of partially melted zones was also been reported in a previous study for welded magnesium [22,23,28–30] and aluminium alloys [31]. Figs. 7 and 8 show the microstructure of the fusion zone, PMZ and base metal for samples GTA welded at a welding speed of 13.33 mm/s and using a current of 200 and 100 A, respectively. In both figures, detailed microphotographs of microstructure changes from the fusion zone to the base metal are presented. As can be seen, the PMZ morphology of the eutectic regions changed from less to more divorced in the direction from the fusion zone to the base metal. Also the width of the local remelted areas decreased in this direction. Near the base metal, the amount (and width) of the melted and resolidified eutectic in the PMZ was comparable to the amount of eutectic in the base metal. This indicated that the rate of dissolution in a solid state was low and once melting starts in

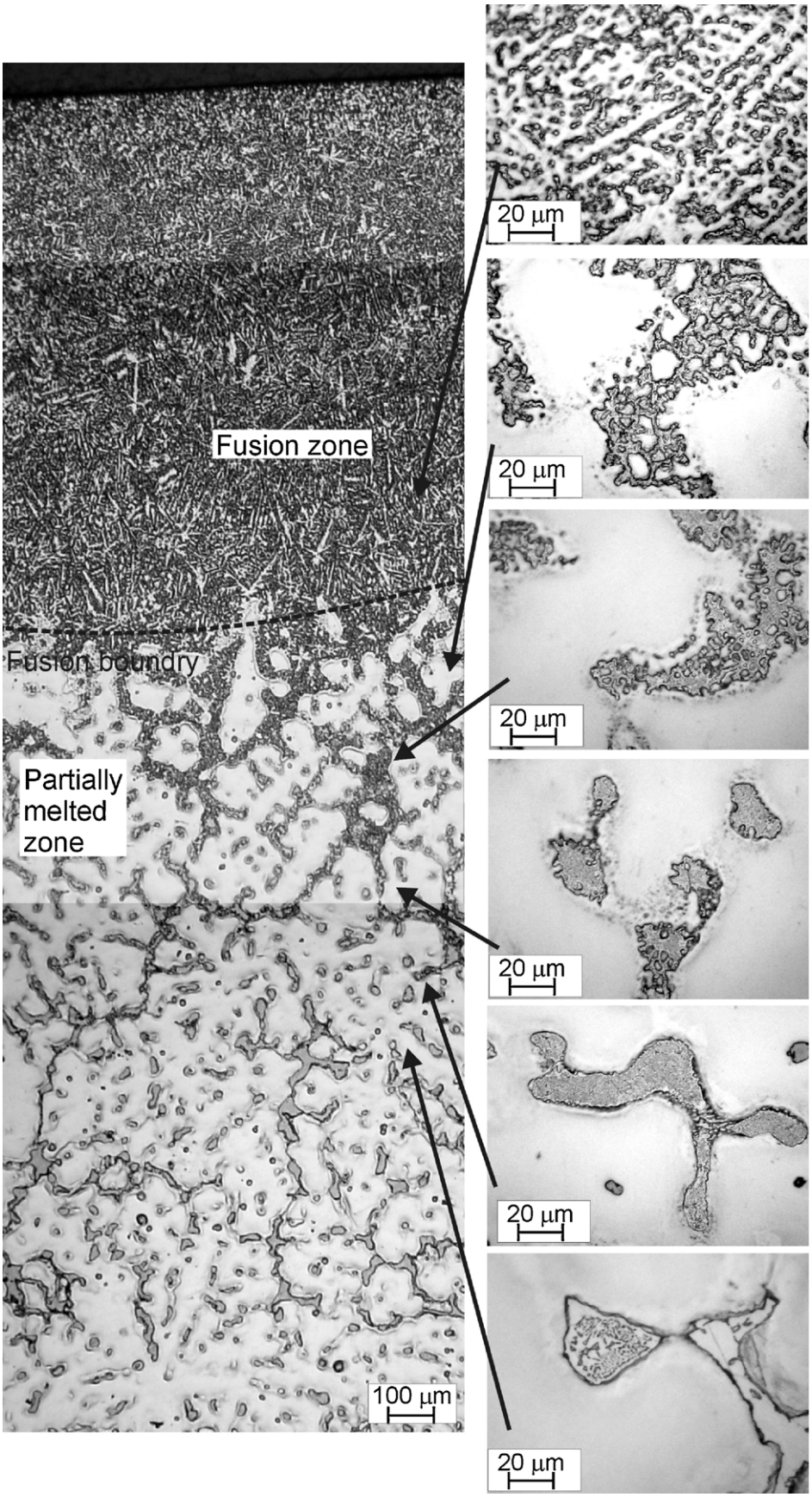

Fig. 7. Microstructure (with detailed microphotographs) of fusion zone, partially melted zone and base metal after GTA welding of AZ91 alloy at 13.3 mm/s welding speed and 200 A current.

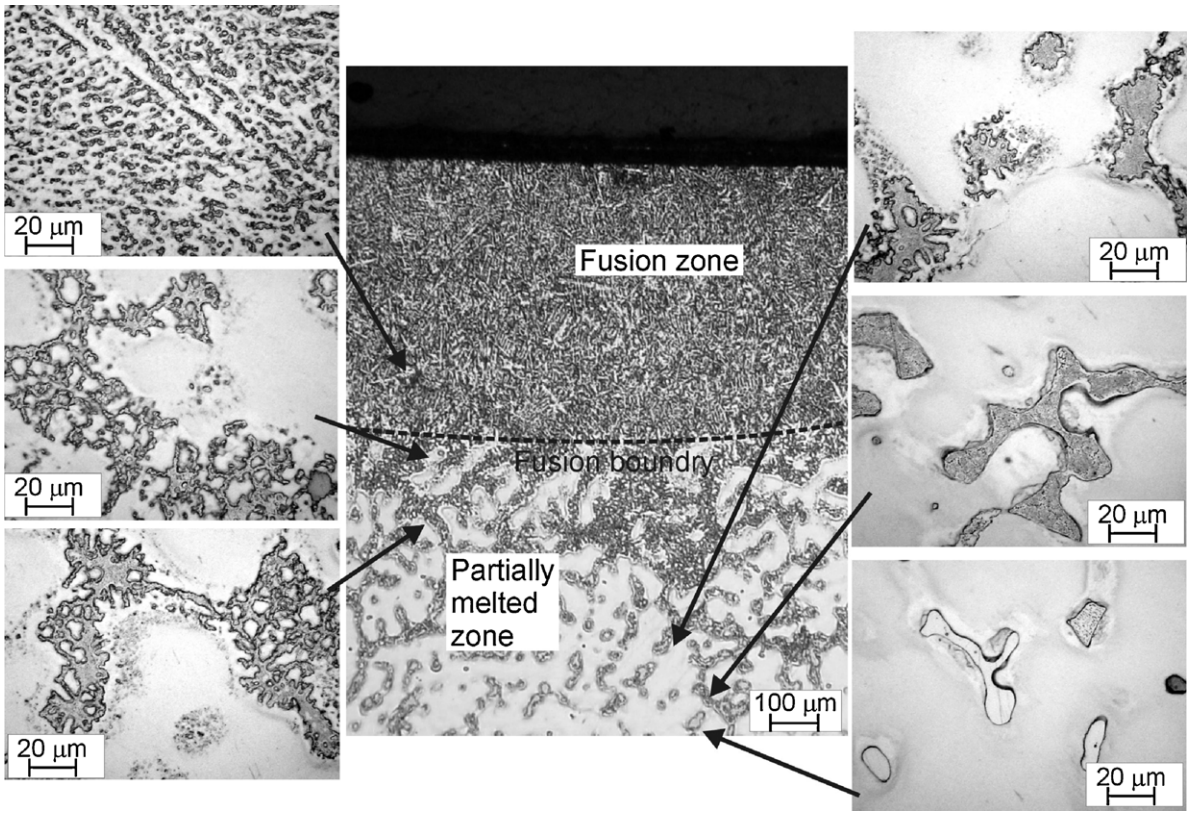

Fig. 8. Microstructure (with detailed microphotographs) of fusion zone, partially melted zone and base metal after GTA welding of AZ91 alloy at 13.3 mm/s welding speed and 100 A current.

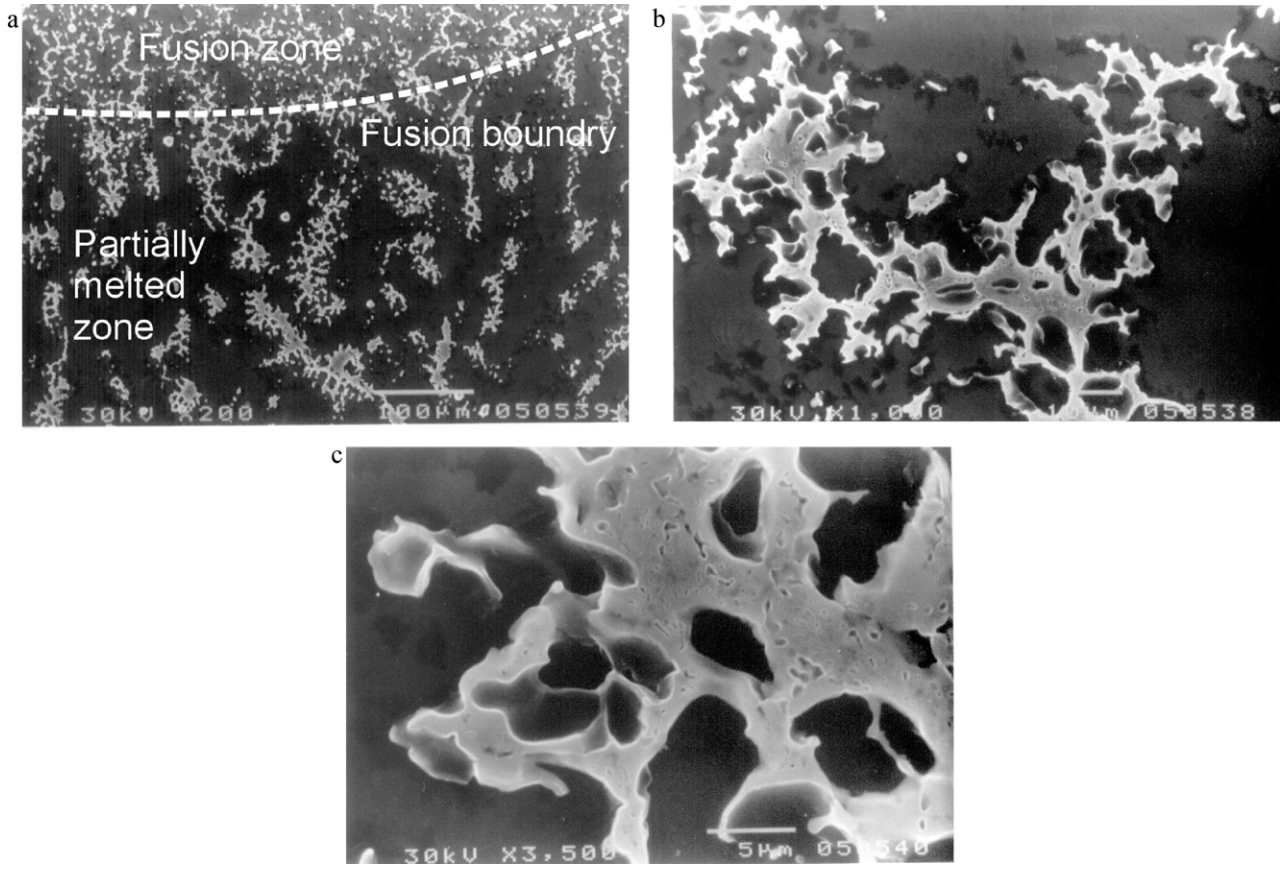

Fig. 9. SEM images of fusion boundary (a) and partially melted zone (b–c) after GTA welding of AZ91 alloy at 3.3 mm/s welding speed and 200 A current.

the PMZ, melting was extensive in the interdendritic regions of the original cast structure. Near the fusion zone, the amount of resolidified areas increased due to a higher temperature during welding. In this region, the remelted areas were visibly wider which indicated that the eutectic α phase surrounding the interdendritical regions was also remelted. Detailed morphology of the PMZ is also presented in Fig. 9. The thermal property of the base metal, energy input and cooling rate of the weld determine the temperature distribution established from the fusion boundary to the base metal. The gradient of temperature distribution also determines the depth of the PMZ. As can be seen from a comparison of Figs. 7 and 8, the depth of the PMZ corresponded to the dimension of the fusion zone.

4. Conclusions

The influence of GTA welding parameters on process efficiencies and microstructure characterization were investigated and the following results were revealed:

1. For the commercial AZ91 magnesium alloy, the arc efficiency values ranged between 0.63 and 0.88 and rose with an increase in welding current and fell with an increase in welding speed.
2. Melting efficiency rises with both an increased welding current and speed to the maximum value of 0.41 using a welding current of 300 A and speed of 13.33 mm/s.
3. The GTA welding process strongly influenced the width and depth of the fusion zone and also the refinement of the microstructure in the fusion zone. The DAS of the remelted material dropped with an increase in welding speed.
4. Due to the low-melting nature of the eutectic in Mg–Al type alloys, the presence of a partially melted zone (PMZ) was formed in a commercial AZ91 magnesium alloy, GTA welded using all the process parameters presented.

References

[1] B.L. Mordike, T. Ebert, Mater. Sci. Eng. A 302 (2001) 37–45.
[2] K.N. Braszczyńska-Malik, A Study on Shaping the Microstructure of Magnesium–Aluminium Alloys, WIPMiFS PCz, Czestochowa, 2005 (in Polish).
[3] S. Kleiner, S. Orgis, O. Beffort, P.J. Uggoqitzer, Adv. Eng. Mater. 9 (2003) 633–658.
[4] A.K. Dahle, Y.C. Lee, P.L. Schaffer, D.H. St. John, J. Light Met. 1 (2001) 61–72.
[5] M.A. Gharghouri, Philos. Mag. 78 (1998) 1137–1149.
[6] T. Zhu, W. Chen, W. Gao, J. Mater. Eng. Perform. 19 (2010) 860–867.
[7] T. Zhu, Z.W. Chen, W. Gao, J. Alloys Compd. 501 (2010) 291–296.
[8] S. Celetto, T.J. Bastow, Acta Mater. 49 (2001) 41–45.
[9] D. Ohno, R. Mirkovic, R. Schmid-Fetzer, Acta Mater. 54 (2005) 3883–3891.
[10] M.A. Gharghouri, G.C. Wetherly, J.D. Embury, J. Root, Philos. Mag. 79 (1999) 1671–1695.
[11] Y.J. Quan, Z.H. Chen, X.S. Gong, Z.H. Yu, Mater. Charact. 59 (2008) 1491–1497.
[12] S.F. Su, J.C. Huang, N.J. Ho, Metall. Mater. Trans. 33A (2002) 1461–1473.
[13] L. Liu, J. Jiang, J. Mater. Process. Technol. 209 (2009) 2864–2870.
[14] S.M. Chowdhury, D.L. Chen, S.D. Bhole, X. Cao, E. Powidajko, D.C. Weckman, Y. Zhou, Mater. Sci. Eng. A 527 (2010) 2951–2961.
[15] K. Abderrazak, W. Kriaa, W.B. Salem, H. Mhiri, G. Lepalec, M. Autic, Opt. Laser Technol. 41 (2009) 470–480.
[16] Y. Jun, G.P. Sun, H.-Y. Wang, S.Q. Jia, S.S. Jia, J. Alloys Compd. 407 (2006) 201–207.
[17] N. Xu, J. Shen, W. Xie, L. Wang, D. Wang, D. Min, Mater. Charact. 61 (2010) 713–719.
[18] J.N. DuPoint, Metall. Mater. Trans. 29B (1998) 932–934.
[19] S. Tashiro, M. Tanaka, M. Nakatani, K. Tani, M. Furubayashi, Surf. Coat. Technol. 201 (2007) 5431–5434.
[20] R.R. Unocic, J.N. DuPont, Metall. Mater. Trans. 35B (2004) 143–152.
[21] M. Marya, G.R. Edwords, S. Liu, Weld. J. (July) (2004) 203–212.
[22] J. Shen, G. You, S. long, F. Pan, Mater. Charact. 59 (2009) 1059–1065.
[23] A. Munitz, C. Cotler, A. Stern, G. Kohn, Mater. Sci. Eng. A 302 (2001) 68–73.
[24] G. Ben-Hamu, D. Eliezer, C.E. Cross, Th. Böllinghaus, Mater. Sci. Eng. A 452–453 (2007) 210–218.
[25] L. Liu, Ch. Dong, Mater. Lett. 60 (2006) 2194–2197.
[26] D. Wenbin, J. Haiyan, Z. Xiaoqin, L. Dehui, Y. Shoushan, J. Alloys Compd. 429 (2007) 233–241.
[27] N. Winzer, P. Xu, S. Bender, T. Gross, W.E.S. Unger, C.E. Cross, Corros. Sci. 51 (2009) 1950–1963.
[28] A. Stern, A. Munitz, J. Mater. Sci. Lett. 18 (1999) 853–855.
[29] T. Zhu, Z.W. Chen, W. Gao, Mater. Sci. Eng. A 416 (2006) 246–252.
[30] T. Zhu, Z.W. Chen, W. Gao, Mater. Charact. 59 (2008) 1550–1558.
[31] K. Prasad Rao, N. Ramanaiah, N. Viswanathan, Mater. Des. 29 (2008) 179–186.